New Roads to the Small-scale Universe: Measurements of the Clustering of Matter with the High-redshift UV Galaxy Luminosity Function

Nashwan Sabti[1] , Julian B. Muñoz[2] , and Diego Blas[3,4]
[1] Department of Physics, King's College London, Strand, London WC2R 2LS, UK; nashwan.sabti@kcl.ac.uk
[2] Harvard-Smithsonian Center for Astrophysics, Cambridge, MA 02138, USA; julianmunoz@cfa.harvard.edu
[3] Grup de Física Teòrica, Departament de Física, Universitat Autònoma de Barcelona, Bellaterra, E-08193 Barcelona, Spain; dblas@ifae.es
[4] Institut de Fisica d'Altes Energies (IFAE), The Barcelona Institute of Science and Technology, Campus UAB, E-08193 Bellaterra (Barcelona), Spain

Abstract

The epochs of cosmic dawn and reionization present promising avenues for understanding the role of dark matter (DM) in our cosmos. The first galaxies that populated the universe during these eras resided in DM halos that were much less massive than their counterparts today. Consequently, observations of such galaxies can provide us with a handle on the clustering of DM in an otherwise currently inaccessible regime. In this work, we use high-redshift UV galaxy luminosity function (UV LF) data from the Hubble Space Telescope to study the clustering properties of DM at small scales. In particular, we present new measurements of the matter power spectrum at wavenumbers $0.5\,\mathrm{Mpc}^{-1} < k < 10\,\mathrm{Mpc}^{-1}$ to roughly 30% precision, obtained after marginalizing over the unknown astrophysics. These new data points cover the uncharted redshift range $4 \leqslant z \leqslant 10$ and encompass scales beyond those probed by cosmic microwave background and large-scale structure observations. This work establishes the UV LF as a powerful tool to probe the nature of DM in a different regime than other cosmological and astrophysical data sets.

Unified Astronomy Thesaurus concepts: Cosmology (343)

1. Introduction

Our exploration of the universe has entered an era where its fundamental properties can be studied with multiple probes in a complementary way. This has allowed us to track its evolution not only from the time of primordial nucleosynthesis down to the present day but also across length scales that span several orders of magnitude (Chabanier et al. 2019). Observations show us a rich evolution of cosmic structures that started off as tiny fluctuations at the time of photon decoupling and hierarchically grew to become the cosmological large-scale structure (LSS) today (Frenk & White 2012). These measurements have been exploited to learn about the mechanisms underlying the formation and growth of structure (Croft et al. 2002; Allen et al. 2011; Kilbinger 2015; Akrami et al. 2020), pointing toward a consistent framework that describes the data in the observed range.

There are, however, still outstanding questions about and challenges to our understanding of structure formation (Bull et al. 2016). Chief among them is the nature of dark matter (DM), which, along with baryons, forms the LSS of our universe. Current data suggest that DM is cold and collisionless at supergalactic scales (Blumenthal et al. 1984; Bertone & Hooper 2018), while at smaller scales, the situation is more uncertain. Alternatives to the cold DM (CDM) paradigm typically show a different behavior at these small scales, making this an interesting regime to probe the properties of DM (Weinberg et al. 2015; Bullock & Boylan-Kolchin 2017; Del Popolo & Le Delliou 2017; de Martino et al. 2020). Another example comes from measurements of the large-scale clustering amplitude σ_8 using observations of the (high-redshift) cosmic microwave background

(CMB) and the (low-redshift) LSS, which appear to be in slight tension with each other (Verde et al. 2019; Di Valentino et al. 2021; Heymans et al. 2021; Perivolaropoulos & Skara 2021).

A promising probe to tackle these open questions is the UV galaxy luminosity function (UV LF). The UV LF captures the abundance of galaxies as a function of their magnitude (or, equivalently, luminosity) at different points in cosmic history and, therefore, contains a wealth of information on the physics of galaxy formation. The past decade has seen the establishment of UV LF catalogs that cover tens of thousands of galaxies during the (pre)reionization era (Atek et al. 2015, 2018; Bouwens et al. 2015, 2017, 2021; Finkelstein et al. 2015; Livermore et al. 2017; Mehta et al. 2017; Ishigaki et al. 2018; Oesch et al. 2018; Rojas-Ruiz et al. 2020). By using the abundance of these galaxies as an indirect probe of the mass function of DM halos, we now have a new handle on the physics of structure formation in this uncharted epoch.

In this Letter, we make use of UV LF data to measure the clustering of matter at small scales ($k \sim 0.5$–$10\,\mathrm{Mpc}^{-1}$) and high redshifts ($z = 4$–10). We show the reach of the UV LF in Figure 1, where it is clear that it presents a unique opportunity to study the state of the universe in a complementary range to local universe probes and CMB observations. The key element of our work is a robust analysis pipeline that carefully marginalizes over astrophysical uncertainties, including the parameters that enter the halo–galaxy connection. Specifically, we use the publicly available likelihood code GALLUMI,[5] which we introduce in our companion paper (Sabti et al. 2022), to perform our analysis. GALLUMI is implemented in the Markov Chain Monte Carlo (MCMC) sampler MontePython (Audren et al. 2013; Brinckmann & Lesgourgues 2019) and can be readily run in conjunction with other data sets. We find that our determination of the matter power spectrum is in agreement

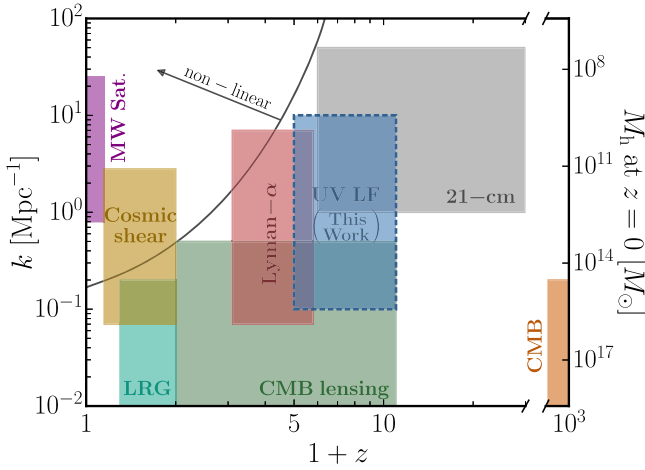---

[5] https://github.com/NNSSA/GALLUMI_public

Figure 1. Illustration of the redshift and wavenumber ranges probed by different types of observations. These include Milky Way (MW) satellites (Banik et al. 2021), cosmic shear (Abbott et al. 2022) and luminous red galaxy (LRG; Chabanier et al. 2019) surveys, CMB (Aghanim et al. 2020a) and CMB lensing (Abazajian et al. 2016) observations, the Lyα forest (Chabanier et al. 2019), and (future) 21 cm (Muñoz et al. 2020) data. The blue region corresponds to our UV LF studies and covers scales and times that are currently inaccessible with other probes. For reference, the right axis is a rough estimate of the corresponding halo masses at redshift $z = 0$, and the region above the black line indicates the nonlinear regime.

with the standard ΛCDM prediction over the entire range of wavenumbers studied here, with an accuracy down to a few tens of percents.

2. UV LF Data

We use galaxy abundance measurements gathered over the last decade with the Hubble Space Telescope (HST). In particular, we will perform our analysis with the data from Oesch et al. (2018) and Bouwens et al. (2021), who compiled search results from the Hubble Legacy Fields and Frontier Fields programs to determine the UV LF over the redshift range $z = 4-10$. These data are based on blank- and parallel-field observations, where galaxies were selected using an object classifier (Bertin & Arnouts 1996), alongside color criteria requirements in selection techniques similar to the Lyman-break dropout method (Steidel et al. 1996). Importantly, galaxies behind lensing clusters were excluded to avoid systematic errors that may arise during the construction of lensing models (Bouwens et al. 2017). The data as is do not account for cosmic variance or the attenuation caused by dust extinction. In addition, since the UV LF is defined in terms of number densities, the data are reported within a certain fiducial cosmology (a flat ΛCDM universe,[6] with Hubble parameter $H_0 = 70 \, \mathrm{km \, s^{-1} \, Mpc^{-1}}$ and matter density parameter $\Omega_m = 0.3$). We correct the UV LF for all three points using the methods described in detail in our companion paper (Sabti et al. 2022). In short, we correct for the Alcock–Paczyński effect (Alcock & Paczynski 1979), use the IRX−β relationship (Meurer et al. 1999) with the calibration from Overzier et al. (2011) to compute the dust attenuation, and impose a minimal error of 20% on each individual data point to account for cosmic variance.

___

[6] Throughout this work, we will fix the total sum of the neutrino masses to $\sum m_\nu = 0.06$ eV. This choice allows us to make comparisons with other analyses but has a negligible impact on our results.

3. Formalism and Models

In order to translate the UV emission and abundance of high-redshift galaxies to cosmological parameters, we need to consider two separate components. The UV LF is defined as

$$\Phi_{\mathrm{UV}} = \frac{dn}{dM_h} \times \frac{dM_h}{dM_{\mathrm{UV}}}, \qquad (1)$$

where the first term (the halo mass function, HMF) mainly depends on cosmology, whereas the second term (the halo–galaxy connection, which links the mass M_h of a DM halo to the absolute magnitude M_{UV} of the galaxy it hosts) depends on astrophysics. Here we implicitly assumed that the halo occupation distribution is unity, i.e., each halo hosts one central galaxy, which is a good approximation at these high redshifts (Bhowmick et al. 2018).

For the HMF, we make use of the Sheth–Tormen mass function, given by Sheth & Tormen (2002),

$$\frac{dn_h}{dM_h} = \frac{\overline{\rho}_m}{M_h} \frac{d \ln \sigma_{M_h}^{-1}}{dM_h} f_{\mathrm{ST}}(\sigma_{M_h}), \qquad (2)$$

with

$$f_{\mathrm{ST}}(\sigma_{M_h}) = A_{\mathrm{ST}} \sqrt{\frac{2a_{\mathrm{ST}}}{\pi}} \left[1 + \left(\frac{\sigma_{M_h}^2}{a_{\mathrm{ST}} \delta_{\mathrm{ST}}^2} \right)^{p_{\mathrm{ST}}} \right] \frac{\delta_{\mathrm{ST}}}{\sigma_{M_h}}$$
$$\times \exp\left(-\frac{a_{\mathrm{ST}} \delta_{\mathrm{ST}}^2}{2\sigma_{M_h}^2} \right), \qquad (3)$$

where $\overline{\rho}_m$ is the average comoving matter energy density, $\sigma_{M_h}^2$ is the variance of the density field smoothed over a mass scale M_h, $A_{\mathrm{ST}} = 0.3222$, $a_{\mathrm{ST}} = 0.707$, $p_{\mathrm{ST}} = 0.3$, and $\delta_{\mathrm{ST}} = 1.686$. The mass variance is defined as

$$\sigma_{M_h}^2 = \int \frac{d^3 k}{(2\pi)^3} W_{M_h}^2(k) T_\zeta^2(k, z) P_\zeta(k), \qquad (4)$$

where W_{M_h} is a window function, and T_ζ and P_ζ are the transfer function and primordial power spectrum of the comoving curvature perturbation ζ, respectively. Unless otherwise stated, we use for the window function a spherical top hat in real space, which in Fourier space reads

$$W_{M_h}(k) = \frac{3 \sin(kR) - 3kR \cos(kR)}{(kR)^3}, \qquad (5)$$

where $R(M_h) = [3M_h/(4\pi\overline{\rho}_m)]^{1/3}$ is the Lagrangian radius (also known as the filter scale). This HMF has been tested against N-body simulations at the redshifts of interest (Lukic et al. 2007; Schneider 2015), including in a specific study of UV LFs (Tacchella et al. 2018).

As for the halo–galaxy connection, we use three astrophysical models to translate M_h into M_{UV}, with differing assumptions about halo accretion, star-to-halo mass ratios, and UV emission. These are detailed in our companion paper (Sabti et al. 2022), where they are shown to produce consistent cosmological results. Here we will simply summarize our fiducial model. The star formation rate (SFR) $\dot{M}_*$ of high-redshift galaxies strongly depends on their host halo mass (Moster et al. 2018; Wechsler & Tinker 2018; Behroozi et al. 2019). In particular, the SFR is expected to peak for galaxies hosted in halos similar to that of the Milky Way and decrease for both smaller and bigger galaxies (Sun & Furlanetto 2016).

This is due to a variety of different baryonic feedback processes, such as active galactic nuclei, supernova shocks, and stellar winds (Kay et al. 2002; Fabian 2012). We model this behavior by assuming a double power-law relation between the SFR of a halo and its accretion rate,

$$\widetilde{f_*} = \frac{\dot{M}_*}{\dot{M}_\mathrm{h}} = \frac{\epsilon_*}{\left(\frac{M_\mathrm{h}}{M_c}\right)^{\alpha_*} + \left(\frac{M_\mathrm{h}}{M_c}\right)^{\beta_*}}, \tag{6}$$

where $\alpha_* \leqslant 0$, $\beta_* \geqslant 0$, $\epsilon_* \geqslant 0$, and $M_c \geqslant 0$ are all free parameters that control the slope of the faint end, the slope of the bright end, the star formation efficiency, and the mass at which the SFR peaks, respectively. In our fiducial model, we keep α_* and β_* independent of redshift, whereas we allow ϵ_* and M_c to evolve as power laws of z (see Sabti et al. 2022 for more details). The SFR and UV luminosity L_UV of a galaxy are related as (Kennicutt 1998; Madau et al. 1998)

$$\dot{M}_* = \kappa_\mathrm{UV} L_\mathrm{UV}, \tag{7}$$

where $\kappa_\mathrm{UV} = 1.15 \times 10^{-28}\, M_\odot\, \mathrm{s}\, \mathrm{erg}^{-1}\, \mathrm{yr}^{-1}$ is a conversion factor obtained from stellar population synthesis models[7] (Madau & Dickinson 2014). The UV luminosity can be expressed in terms of the absolute magnitude through (Oke & Gunn 1983)

$$\log_{10}\left(\frac{L_\mathrm{UV}}{\mathrm{erg}\, \mathrm{s}^{-1}}\right) = 0.4\,(51.63 - M_\mathrm{UV}). \tag{8}$$

As a final step, we require an expression for the halo accretion rate $\dot{M}_h$. For this purpose, we turn to the extended Press–Schechter formalism, which provides a semianalytical description for $\dot{M}_\mathrm{h}$ that agrees very well with the output of N-body simulations (Correa et al. 2015). Within this formalism, the halo mass grows exponentially during matter domination and follows a power-law behavior with z at lower redshifts due to dark energy domination. The accretion rate is given by Neistein & van den Bosch (2006) and Correa et al. (2015):

$$\dot{M}_\mathrm{h} = -\sqrt{\frac{2}{\pi}}\,\frac{(1+z)H(z)M_\mathrm{h}}{\sqrt{\sigma^2_{M_\mathrm{h}}(Q) - \sigma^2_{M_\mathrm{h}}}}\,\frac{1.686}{D^2(z)}\,\frac{\mathrm{d}D(z)}{\mathrm{d}z}. \tag{9}$$

In this equation, $D(z)$ is the linear growth factor, and $\sigma^2_{M_\mathrm{h}}(Q) \equiv \sigma^2(M_\mathrm{h}/Q)$ is the rescaled mass variance, where Q is a free parameter. This latter quantity is calibrated with N-body simulations, and we allow it to vary within the range $Q = 1.5\text{–}2.5$ found by previous works (Neistein & van den Bosch 2006; Schneider et al. 2021).

In summary, we use Equations (6) and (9) to obtain the SFR as a function of halo mass M_h, including scatter as described in Sabti et al. (2022). The SFR is then expressed in terms of a UV magnitude using Equations (7) and (8). From this, we can straightforwardly compute the UV LF in Equation (1). We show our best-fit model in Figure 2, which is in good agreement with the HST data.

4. Clustering Amplitude

The raw UV LF data roughly cover absolute magnitudes from $M_\mathrm{UV} = -23$ to -16, which correspond to typical halo

---

[7] This parameter could be varied in our analysis, though it is fully degenerate with ϵ_*.
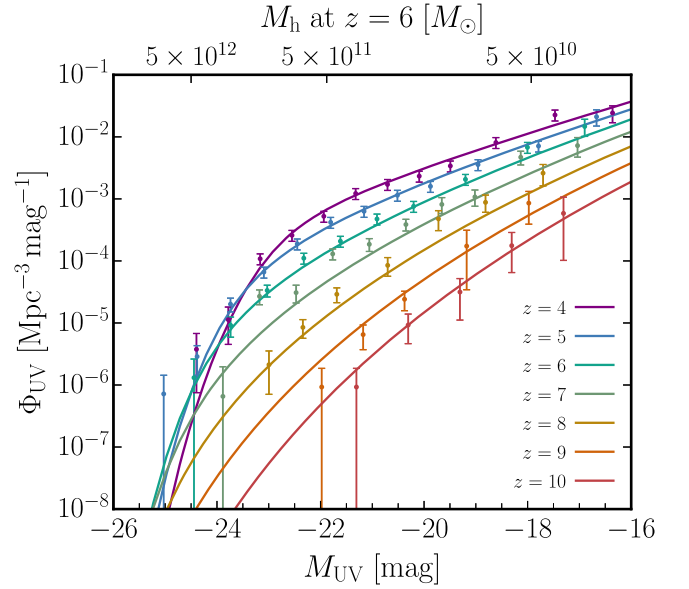

Figure 2. Global fit of our fiducial model to the UV LF data from the HST (Oesch et al. 2018; Bouwens et al. 2021). The data points shown here are corrected for dust attenuation and the Alcock–Paczyński effect. For illustration purposes, the top axis shows the corresponding halo masses at redshift $z = 6$ within our best-fit model.

masses of $M_\mathrm{h} \sim 10^{10}\text{–}10^{12}\, M_\odot$ at redshift $z = 6$ (assuming our fiducial model; see also Figure 2). While these halos are rather common today, at high redshifts, the high-mass (bright) end of the UV LF is in the exponential tail of the HMF and thus particularly sensitive to changes in the amplitude of clustering. We will now quantify what clustering information can be extracted from the UV LFs. A full description of our analysis pipeline is provided in our companion paper (Sabti et al. 2022).

We start by measuring the large-scale clustering amplitude $\sigma_8 \equiv \sigma(R = 8/h\, \mathrm{Mpc})$, which allows us to contextualize our results with other clustering measurements at both lower and higher redshifts. We show our posteriors for σ_8 and Ω_m in Figure 3, along with those from CMB, cosmic shear, and galaxy-clustering observations. After marginalizing over all cosmological and astrophysical parameters, we obtain a measurement of σ_8 that reads

$$\sigma_8 = 0.76^{+0.12}_{-0.14} \tag{10}$$

at 68% CL. We thus find that UV LFs can measure σ_8 within $\sim15\%$ uncertainty, a factor of a few less constraining than what is obtained with the other data sets, though independent of them (see also Sahlén & Zackrisson 2021 for a recent study).

A key advantage of the UV LFs is their ability to probe smaller halo masses, where deviations from CDM may first appear. Thus, we now turn to measuring the amplitude of matter fluctuations at small scales. Rather than focusing on any particular non-CDM model, we will obtain model-agnostic measurements of the matter power spectrum at large wavenumbers k, which can then be applied to a wide range of models. We will follow a simple approach in doing so. We divide the power spectrum into four bins, whose amplitudes $a_\mathrm{s,i}$ we will vary as
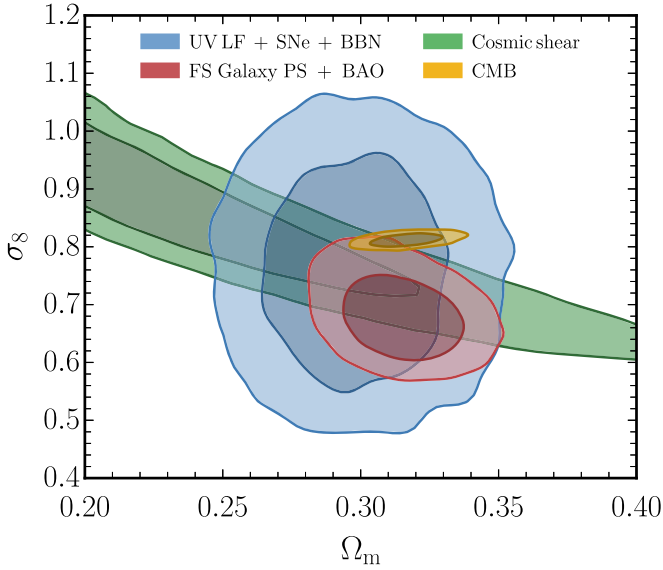
Figure 3. Posteriors for the large-scale clustering amplitude σ_8 versus the matter density parameter Ω_m. The inner (outer) contours represent the 68% (95%) confidence levels. Our result (in blue, where we used HST UV LF data (Oesch et al. 2018; Bouwens et al. 2021), Pantheon supernovae distance moduli determinations (Jones et al. 2018; Scolnic et al. 2018), and baryon density inferences from primordial-abundance measurements (Pisanti et al. 2021)) is shown along with the KV450+DES-Y1 cosmic shear analysis from Joudaki et al. (2020; green), the BOSS full-shape galaxy power spectra and BAO analysis from Philcox et al. (2020; red), and the Planck CMB analysis from Aghanim et al. (2020; yellow). Note that the supernova and primordial-abundance data used in our analysis here only constrain Ω_m and ω_b, respectively, and do not contain any information on σ_8. In all cases, the total sum of the neutrino masses is fixed to $\sum m_\nu = 0.06$ eV.

$$P(k) = \begin{cases} P_k^{\Lambda CDM} & \text{if } k < 0.5 \text{ Mpc}^{-1} \\ a_{s,2} P_k^{\Lambda CDM} & \text{if } 0.5 \leqslant k < 2.25 \text{ Mpc}^{-1} \\ a_{s,3} P_k^{\Lambda CDM} & \text{if } 2.25 \leqslant k < 10 \text{ Mpc}^{-1} \\ a_{s,4} P_k^{\Lambda CDM} & \text{if } k \geqslant 10 \text{ Mpc}^{-1} \end{cases} \quad (11)$$

where $P_k^{\Lambda CDM}$ is the matter power spectrum in ΛCDM. We emphasize that the amplitudes $a_{s,i}$ are relative to the overall scalar amplitude A_s, which is the amplitude of P_k^{Λ}CDM. We use Planck 2018 TTTEEE+lowE+lensing data (Aghanim et al. 2020b) to constrain the large-scale behavior of the power spectrum (and thus A_s, which also acts as the amplitude of the first bin). The bins have been chosen so that CMB data can mainly probe the first one ($k < 0.5$ Mpc^{-1}; see, e.g., Chabanier et al. 2019), whereas the last one, at very small scales ($k > 10$ Mpc^{-1}), will not be well measured even by the UV LFs. We divide the intermediate range 0.5 Mpc$^{-1} < k < 10$ Mpc^{-1} into two bins, whose amplitudes we can measure with the UV LFs.[8] The amplitudes $a_{s,i}$ (with fiducial values of unity) are varied independently from 10^{-9} to 10^9, assuming a log-flat prior.

Since we essentially allow for a cutoff in the matter power spectrum, we need to be careful with our choice of the window function in Equation (4). Using a real-space top-hat window function with a truncated power spectrum can lead to σ_{M_h} to

---

[8] Using more bins would weaken our constraints, since the amplitudes of the bins are strongly correlated with each other. Two bins is therefore a reasonable compromise between obtaining strong constraints and resolving the k behavior.
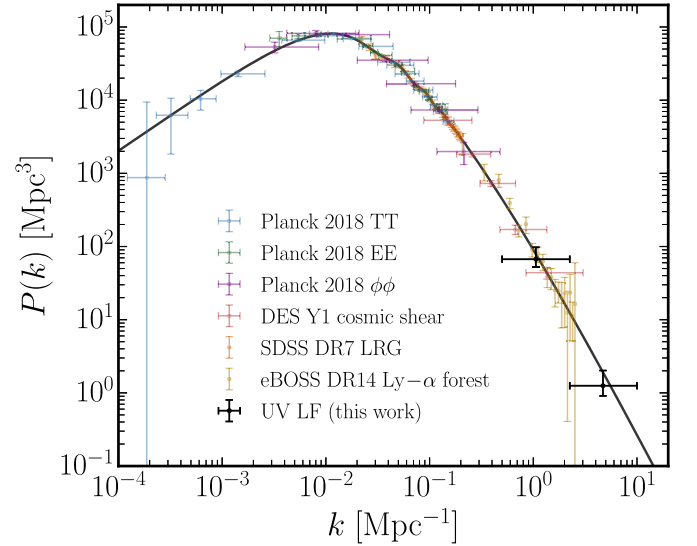

Figure 4. Measurements of the matter power spectrum (of DM and baryons only) linearly extrapolated to redshift $z = 0$. The two black data points are the results of this work and obtained with the UV LF data from Oesch et al. (2018) and Bouwens et al. (2021), where we imposed a prior from Planck 2018 CMB observations (TTTEEE+lowE+lensing) to constrain the small-k behavior. The colored data points represent measurements using Planck 2018 CMB (Aghanim et al. 2020), DES cosmic shear (Troxel et al. 2018), SDSS galaxy clustering (Reid et al. 2010), and SDSS Lyα (Abolfathi et al. 2018) data (see Chabanier et al. 2019 for more details). The black line is the prediction within ΛCDM using the best-fit values from Planck 2018 (Aghanim et al. 2020). All uncertainties in this figure are at 68% CL.

keep increasing even for masses below the cutoff scale (Benson et al. 2013; Schneider 2015). This is a well-known issue and can be circumvented by using a sharp-k window function (Bertschinger 2006; Schneider et al. 2013),

$$W_{M_h}(k) = \Theta(1 - kR), \quad (12)$$

where Θ is the Heaviside step function. A side effect of using the sharp-k filter is that the relation between halo mass and filter scale R is not well defined. We follow Schneider (2015, 2018) and introduce a new parameter, $c = 2.5$, in the definition of the halo mass $M_h = 4\pi \bar{\rho}_m (cR)^3/3$, which is found to well fit their simulations with cold, warm, and fuzzy DM. Following these same references, one would have to set a_{ST} in Equation (3) to unity, as the new variable c takes over its role in calibrating the HMF. We conservatively allow for additional freedom in the HMF by varying a_{ST} between 0.9 and 1, which ensures that the CDM mass function is always included as a prediction in our model.

We use our fiducial UV LF model and run our analysis with the 2021 HST data compiled in Bouwens et al. (2021), in conjunction with the Planck 2018 TTTEEE+lowE+lensing data (Aghanim et al. 2020b). We present our main results in Figure 4. This figure displays our measurement of the small-scale matter power spectrum alongside data points from a number of other probes (Chabanier et al. 2019). The black data points are obtained by computing the power spectrum at the center of each bin (as in Equation (11)) and marginalizing over all cosmological and astrophysical parameters. We measure the small-scale amplitudes (relative to ΛCDM) in Equation (11) to be $a_{s,2} = 0.93^{+0.34}_{-0.25}$ and $a_{s,3} = 0.66^{+0.43}_{-0.17}$ at 68% CL. Our UV LF analysis is able to reach smaller scales than other current cosmological probes, which provides a new lamppost to

understand the clustering properties of DM (Jethwa et al. 2018; Banik et al. 2021; Nadler et al. 2019 and 2020; Gilman et al. 2020; Hsueh et al. 2020; Enzi et al. 2021; Nadler et al. 2021a, 2021b; Newton et al. 2021). We find that the matter power spectrum is consistent with the theoretical prediction of a standard ΛCDM cosmology up to $k = 10\,\text{Mpc}^{-1}$, which disfavors alternatives that suppress power at these scales, such as warm (Bode et al. 2001; Boyarsky et al. 2019) or fuzzy (Marsh 2016; Hui 2021) DM.

5. Conclusions

The UV LFs capture a wealth of information about the universe around the epoch of cosmic reionization. In addition to shedding light on the astrophysics of this interesting era, we have shown that the same data can be used to measure the clustering of matter at smaller scales and higher redshifts than currently accessible. In particular, here we used UV LF data from observations of the HST (Oesch et al. 2018; Bouwens et al. 2021) to derive new constraints on the matter power spectrum at wavenumbers $k = 0.5\text{–}10\,\text{Mpc}^{-1}$ and redshifts $z = 4\text{–}10$. In this range, DM halo collapse is still not in the deep nonlinear regime (i.e., the satellite fraction is negligible), and the dust attenuation only affects the brightest galaxies, which simplifies the modeling. Throughout the text, we focused on our fiducial model for the halo–galaxy connection. As a cross-check, we have performed the same study using the two other astrophysical models detailed in our companion paper (Sabti et al. 2022) and found good agreement among the three models due to our marginalization over the astrophysical parameters. In addition, we have used an alternative determination of the UV LFs from Finkelstein et al. (2015) and found consistent results for σ_8 and the amplitudes in Equation (11) within roughly 1σ and 2σ, respectively. Finally, we find that using the Reed mass function or different calibrations for the dust extinction does not alter our conclusions significantly, as in both cases, mainly the bright end of the UV LF (where the Poisson errors are already large) is affected; see Sabti et al. (2022). We note that if a cutoff in the UV LF were detected, one would have to proceed with caution. For example, one could do a careful model comparison (e.g., with a Bayesian method) to determine whether the data prefer a DM cutoff over an astrophysical one, given their different shapes.

Our analysis here establishes the UV LF as a powerful cosmic probe of small-scale structure, providing us with valuable insights beyond the frameworks of specific DM or inflationary models (Schultz et al. 2014; Bozek et al. 2015; Chevallard et al. 2015; Dayal et al. 2015; Corasaniti et al. 2017; Menci et al. 2017, 2018; Yoshiura et al. 2020; Rudakovskyi et al. 2021; Sabti et al. 2021). Together with current large-scale cosmological data sets, the UV LF expands our knowledge of the clustering of matter to cover nearly 5 orders of magnitude in scale ($10^{-4}\,\text{Mpc}^{-1} < k < 10\,\text{Mpc}^{-1}$; see Figure 4). In the near future, the James Webb Space Telescope (Gardner et al. 2006) and Nancy Grace Roman Space Telescope (Spergel et al. 2015) will not only observe galaxies at higher redshifts than covered by current HST data but also probe halos with smaller masses. This provides us with an exciting outlook on the study of the growth and clustering of matter.

ORCID iDs

Nashwan Sabti https://orcid.org/0000-0002-7924-546X
Julian B. Muñoz https://orcid.org/0000-0002-8984-0465
Diego Blas https://orcid.org/0000-0003-2646-0112

References

Abazajian, K. N., Adshead, P., Ahmed, Z., et al. 2016, arXiv:1610.02743
Abbott, T. M. C., Aguena, M., Alarcon, A., et al. 2022, PhRvD, 105, 023520
Abolfathi, B., Aguado, D. S., Aguilar, G., et al. 2018, ApJS, 235, 42
Aghanim, N., Akrami, Y., Arroja, F., et al. 2020a, A&A, 641, A1
Aghanim, N., Akrami, Y., Ashdown, M., et al. 2020, A&A, 641, A6
Aghanim, N., Akrami, Y., Ashdown, M., et al. 2020b, A&A, 641, A5
Akrami, Y., Arroja, F., Ashdown, M., et al. 2020, A&A, 641, A1
Alcock, C., & Paczynski, B. 1979, Natur, 281, 358
Allen, S. W., Evrard, A. E., & Mantz, A. B. 2011, ARA&A, 49, 409
Atek, H., Richard, J., Kneib, J.-P., & Schaerer, D. 2018, MNRAS, 479, 5184
Atek, H., Richard, J., Jauzac, M., et al. 2015, ApJ, 814, 69
Audren, B., Lesgourgues, J., Benabed, K., & Prunet, S. 2013, JCAP, 1302, 001
Banik, N., Bovy, J., Bertone, G., Erkal, D., & de Boer, T. J. L. 2021, JCAP, 10, 043
Behroozi, P., Wechsler, R. H., Hearin, A. P., & Conroy, C. 2019, MNRAS, 488, 3143
Benson, A. J., Farahi, A., Cole, S., et al. 2013, MNRAS, 428, 1774
Bertin, E., & Arnouts, S. 1996, A&AS, 117, 393
Bertone, G., & Hooper, D. 2018, RvMP, 90, 045002
Bertschinger, E. 2006, PhRvD, 74, 063509
Bhowmick, A. K., Campbell, D., Di Matteo, T., & Feng, Y. 2018, MNRAS, 480, 3177
Blas, D., Lesgourgues, J., & Tram, T. 2011, JCAP, 07, 034
Blumenthal, G. R., Faber, S. M., Primack, J. R., & Rees, M. J. 1984, Natur, 311, 517
Bode, P., Ostriker, J. P., & Turok, N. 2001, ApJ, 556, 93
Bouwens, R. J., Oesch, P. A., Illingworth, G. D., Ellis, R. S., & Stefanon, M. 2017, ApJ, 843, 129
Bouwens, R. J., Oesch, P. A., Stefanon, M., et al. 2021, AJ, 162, 47
Bouwens, R., Illingworth, G. D., Oesch, P. A., et al. 2015, ApJ, 803, 34
Boyarsky, A., Drewes, M., Lasserre, T., Mertens, S., & Ruchayskiy, O. 2019, PrPNP, 104, 1
Bozek, B., Marsh, D. J. E., Silk, J., & Wyse, R. F. G. 2015, MNRAS, 450, 209
Brinckmann, T., & Lesgourgues, J. 2019, PDU, 24, 100260
Bull, P., Akrami, Y., Adamek, J., et al. 2016, PDU, 12, 56
Bullock, J. S., & Boylan-Kolchin, M. 2017, ARA&A, 55, 343
Chabanier, S., Millea, M., & Palanque-Delabrouille, N. 2019, MNRAS, 489, 2247
Chevallard, J., Silk, J., Nishimichi, T., et al. 2015, MNRAS, 446, 3235
Corasaniti, P., Agarwal, S., Marsh, D., & Das, S. 2017, PhRvD, 95, 083512
Correa, C. A., Wyithe, J. S. B., Schaye, J., & Duffy, A. R. 2015, MNRAS, 450, 1514
Croft, R. A. C., Weinberg, D. H., Bolte, M., et al. 2002, ApJ, 581, 20
Dayal, P., Mesinger, A., & Pacucci, F. 2015, ApJ, 806, 67
de Martino, I., Chakrabarty, S. S., Cesare, V., et al. 2020, Univ, 6, 107

Del Popolo, A., & Le Delliou, M. 2017, Galax, 5, 17
Di Valentino, E., Anchordoqui, L. A., Akarsu, Ö., et al. 2021, APh, 131, 102604
Enzi, W., Murgia, R., Newton, O., et al. 2021, MNRAS, 506, 4
Fabian, A. C. 2012, ARA&A, 50, 455
Finkelstein, S. L., Ryan Jr., R. E., Papovich, C., et al. 2015, ApJ, 810, 71
Frenk, C. S., & White, S. D. M. 2012, AnP, 524, 507
Gardner, J. P., Mather, J. C., Clampin, M., et al. 2006, SSRv, 123, 485
Gilman, D., Birrer, S., Nierenberg, A., et al. 2020, MNRAS, 491, 6077
Heymans, C., Tröster, T., Asgari, M., et al. 2021, A&A, 646, A140
Hsueh, J.-W., Enzi, W., Vegetti, S., et al. 2020, MNRAS, 492, 3047
Hui, L. 2021, ARA&A, 59, 42
Ishigaki, M., Kawamata, R., Ouchi, M., et al. 2018, ApJ, 854, 73
Jethwa, P., Erkal, D., & Belokurov, V. 2018, MNRAS, 473, 2060
Jones, D. O., Scolnic, D. M., Riess, A. G., et al. 2018, ApJ, 857, 51
Joudaki, S., Hildebrandt, H., Traykova, D., et al. 2020, A&A, 638, L1
Kay, S. T., Pearce, F. R., Frenk, C. S., & Jenkins, A. 2002, MNRAS, 330, 113
Kennicutt, R. C. J. 1998, ARA&A, 36, 189
Kilbinger, M. 2015, RPPh, 78, 086901
Lesgourgues, J. 2011, arXiv:1104.2932
Livermore, R., Finkelstein, S., & Lotz, J. 2017, ApJ, 835, 113
Lukic, Z., Heitmann, K., Habib, S., Bashinsky, S., & Ricker, P. M. 2007, ApJ, 671, 1160
Madau, P., & Dickinson, M. 2014, ARA&A, 52, 415
Madau, P., Pozzetti, L., & Dickinson, M. 1998, ApJ, 498, 106
Marsh, D. J. E. 2016, PhR, 643, 1
Mehta, V., Scarlata, C., Rafelski, M., et al. 2017, ApJ, 838, 29
Menci, N., Grazian, A., Lamastra, A., et al. 2018, ApJ, 854, 1
Menci, N., Merle, A., Totzauer, M., et al. 2017, ApJ, 836, 61
Meurer, G. R., Heckman, T. M., & Calzetti, D. 1999, ApJ, 521, 64
Moster, B. P., Naab, T., & White, S. D. M. 2018, MNRAS, 477, 1822
Muñoz, J. B., Dvorkin, C., & Cyr-Racine, F.-Y. 2020, PhRvD, 101, 063526
Nadler, E. O., Birrer, S., Gilman, D., et al. 2021a, ApJ, 917, 7
Nadler, E. O., Drlica-Wagner, A., Bechtol, K., et al. 2021b, PhRvL, 126, 091101
Nadler, E. O., Gluscevic, V., Boddy, K. K., & Wechsler, R. H. 2019, ApJL, 878, L32
Nadler, E. O., Gluscevic, V., Boddy, K. K., & Wechsler, R. H. 2020, ApJL, 897, L46
Neistein, E., & van den Bosch, F. C. 2006, MNRAS, 372, 933
Newton, O., Leo, M., Cautun, M., et al. 2021, JCAP, 08, 062
Oesch, P. A., Bouwens, R. J., Illingworth, G. D., Labbé, I., & Stefanon, M. 2018, ApJ, 855, 105
Oke, J. B., & Gunn, J. E. 1983, ApJ, 266, 713
Overzier, R., Heckman, T. M., Wang, J., et al. 2011, ApJL, 726, L7
Perivolaropoulos, L., & Skara, F. 2021, arXiv:2105.05208
Philcox, O. H. E., Ivanov, M. M., Simonović, M., & Zaldarriaga, M. 2020, JCAP, 05, 032
Pisanti, O., Mangano, G., Miele, G., & Mazzella, P. 2021, JCAP, 04, 020
Reid, B. A., Percival, W. J., Eisenstein, D. J., et al. 2010, MNRAS, 404, 60
Rojas-Ruiz, S., Finkelstein, S. L., Bagley, M. B., et al. 2020, ApJ, 891, 146
Rudakovskyi, A., Mesinger, A., Savchenko, D., & Gillet, N. 2021, MNRAS, 507, 3046
Sabti, N., Muñoz, J. B., & Blas, D. 2021, JCAP, 01, 010
Sabti, N., Muñoz, J. B., & Blas, D. 2022, PhRvD, 105, 043518
Sahlén, M., & Zackrisson, E. 2021, arXiv:2105.05098
Schneider, A. 2015, MNRAS, 451, 3117
Schneider, A. 2018, PhRvD, 98, 063021
Schneider, A., Giri, S. K., & Mirocha, J. 2021, PhRvD, 103, 083025
Schneider, A., Smith, R. E., & Reed, D. 2013, MNRAS, 433, 1573
Schultz, C., Oñorbe, J., Abazajian, K. N., & Bullock, J. S. 2014, MNRAS, 442, 1597
Scolnic, D. M., Jones, D. O., Rest, A., et al. 2018, ApJ, 859, 101
Sheth, R. K., & Tormen, G. 2002, MNRAS, 329, 61
Spergel, D., Gehrels, N., Baltay, C., et al. 2015, arXiv:1503.03757
Steidel, C. C., Giavalisco, M., Pettini, M., Dickinson, M., & Adelberger, K. L. 1996, ApJL, 462, L17
Sun, G., & Furlanetto, S. R. 2016, MNRAS, 460, 417
Tacchella, S., Bose, S., Conroy, C., Eisenstein, D. J., & Johnson, B. D. 2018, ApJ, 868, 92
Troxel, M. A., MacCrann, N., Zuntz, J., et al. 2018, PhRvD, 98, 043528
Verde, L., Treu, T., & Riess, A. G. 2019, NatAs, 3, 891
Wechsler, R. H., & Tinker, J. L. 2018, ARA&A, 56, 435
Weinberg, D. H., Bullock, J. S., Governato, F., Kuzio de Naray, R., & Peter, A. H. G. 2015, PNAS, 112, 12249
Yoshiura, S., Oguri, M., Takahashi, K., & Takahashi, T. 2020, PhRvD, 102, 083515

6